

# Structural Studies and Magnetic Properties of Polymeric Ladder-Type Compounds $\{\text{Ln}_2[\text{Ni}(\text{opba})]_3\} \cdot \text{S}$ (Ln = Lanthanide Element; opba = *o*-Phenylenebis(oxamato), S = Solvent Molecules)

Myrtil L. Kahn,<sup>†</sup> Pierre Lecante,<sup>‡</sup> Marc Verelst,<sup>‡</sup> Corine Mathonière,<sup>\*,†</sup> and Olivier Kahn<sup>†,§</sup>

*Institut de Chimie de la Matière Condensée de Bordeaux, Laboratoire des Sciences Moléculaires, UPR CNRS NE 9048, 33608 Pessac, France, and Centre d'Elaboration de Matériaux et d'Etudes Structurales, UPR CNRS NE 8011, BP 4743, 29 Rue Jeanne Marvig, 31055 Toulouse, France*

Received March 20, 2000. Revised Manuscript Received July 17, 2000

The compounds of formula  $\{\text{Ln}_2[\text{Ni}(\text{opba})]_3\} \cdot \text{S}$  (opba being *o*-phenylenebis(oxamato), Ln lanthanide<sup>III</sup> ions, and S solvents molecules) have been structurally and magnetically characterized for Ln = La, Ce, Pr, Nd, Gd, Tb, Dy, Ho, and Er. These compounds crystallize poorly, and structural information has been obtained from EXAFS and wide-angle X-ray scattering (WAXS) techniques. The EXAFS studies have shown that the Ni site may adopt square planar geometry (with a spin  $S_{\text{Ni}} = 0$ ) or octahedral geometry (with  $S_{\text{Ni}} = 1$ ). The compounds are orange when the Ni sites are mostly square planar or green for Ni sites mostly octahedral. The WAXS studies have shown that the compounds present the same ladder-like motif as that previously described for  $\text{Tm}_2[\text{Cu}(\text{opba})]_3 \cdot 4\text{H}_2\text{O} \cdot 10\text{DMF}$ . The magnetic properties of the compounds with magnetic octahedral Ni sites have been studied and compared with those of the  $\{\text{Ln}_2[\text{Zn}(\text{opba})]_3\} \cdot \text{S}$  series for each Ln ion. This comparison allows us to determine the nature of interactions in  $\text{Ln}^{\text{III}}-\text{Ni}^{\text{II}}$  pairs. It is clearly established that the interaction is ferromagnetic when  $\text{Ln}^{\text{III}}$  is  $\text{Gd}^{\text{III}}$ ,  $\text{Tb}^{\text{III}}$ ,  $\text{Dy}^{\text{III}}$ , and perhaps  $\text{Ho}^{\text{III}}$ . On the contrary, the interaction seems to be antiferromagnetic for  $\text{Ln}^{\text{III}} = \text{Ce}^{\text{III}}$ ,  $\text{Pr}^{\text{III}}$ ,  $\text{Nd}^{\text{III}}$ ,  $\text{Er}^{\text{III}}$ . These results are discussed with those obtained recently in  $\text{Ln}^{\text{III}}-\text{Cu}^{\text{II}}$  pairs.

## Introduction

In the 1980s, the ferromagnetic interaction between  $\text{Gd}^{\text{III}}$  and  $\text{Cu}^{\text{II}}$  ions was clearly reported in molecular compounds.<sup>1</sup> This result was in contrast to what may be expected between  $\text{Gd}^{\text{III}}(4f^7)$  and  $\text{Cu}^{\text{II}}(3d^9)$  ions where the magnetic orbitals overlap, leading in principle to an antiferromagnetic interaction. Two mechanisms were proposed. The first one suggested by Gatteschi et al.<sup>2</sup> is based on spin polarization effects. The second interpretation given by Kahn et al.<sup>3</sup> considers the interaction between ground-state and charge-transfer configurations. Whatever the mechanism, the parallel alignment of  $\text{Gd}^{\text{III}}$  and  $\text{Cu}^{\text{II}}$  spins with respect to the Hund rule occurs. In the past decade, several  $\text{Gd}^{\text{III}}-\text{Cu}^{\text{II}}$  pairs have been structurally and magnetically characterized. In most cases, the  $\text{Gd}^{\text{III}}-\text{Cu}^{\text{II}}$  interaction was found to be

ferromagnetic.<sup>4</sup> To the best of our knowledge, only one example of a  $\text{Gd}^{\text{III}}-\text{Cu}^{\text{II}}$  antiferromagnetic interaction has been reported by Costes et al.<sup>5</sup> In these examples, with the  $\text{Gd}^{\text{III}}$  having a pure spin ground state, the magnetic properties can be interpreted with an Heisenberg Hamiltonian of type  $J\mathbf{S}_{\text{Gd}} \cdot \mathbf{S}_{\text{Cu}}$ , where  $J$  is the interaction parameter (positive for a ferromagnetic interaction) and  $\mathbf{S}_{\text{Gd}}$  and  $\mathbf{S}_{\text{Cu}}$  are the spin operators for Gd and Cu ions, respectively. For other paramagnetic rare earth ions, noted  $\text{Ln}^{\text{III}}$ , the situation is more complicated because of the presence of an orbital contribution in addition to the spin operator. Indeed, the spectrum of the low-lying states of a rare earth ion consists of Stark sublevels arising from the split of the spectroscopic levels  $2S+1L_J$  by the crystal field perturbation (up to  $2J+1$  if  $n$  is even and  $J+1/2$  if  $n$  is odd for a  $4f^n$  configuration). The magnetic properties of a system where the lanthanide ion is in interaction with other paramagnetic species are the superposition of two phenomena: the thermal depopulation of the Stark sublevels of the rare earth ion and the magnetic

\* To whom correspondence should be addressed.

<sup>†</sup> Laboratoire des Sciences Moléculaires.

<sup>‡</sup> Centre d'Elaboration de Matériaux et d'Etudes Structurales.

<sup>§</sup> Deceased December 8, 1999.

(1) (a) Bencini, A.; Benelli, C.; Caneschi, A.; Carlin, R.; Dei, A.; Gatteschi, D. *J. Am. Chem. Soc.* **1985**, *107*, 8128. (b) Bencini, A.; Benelli, C.; Caneschi, A.; Dei, A.; Gatteschi, D. *Inorg. Chem.* **1986**, *25*, 572. (c) Matsumoto, N.; Sakamoto, M.; Tamaki, H.; Okawa, H. *Chem. Lett.* **1990**, 853.

(2) Benelli, C.; Caneschi, A.; Guillou, O.; Gatteschi, D.; Pardi, L. *Inorg. Chem.* **1990**, *29* 1750.

(3) Kahn, O.; Guillou, O. *Res. Front. Magnetochem.* **1993**, 179.

(4) (a) Costes, J.-P.; Dahan, F.; Dupuis, A.; Laurent, J.-P. *Inorg. Chem.* **1997**, *36*, 3429. (b) Ramade, I.; Kahn, O.; Jeannin, Y.; Robert, F. *Inorg. Chem.* **1998**, *37*, 4712. (c) Kahn, M. L.; Rajendiran, T. M.; Jeannin, Y.; Mathonière, C.; Kahn O. *C. R. Acad. Sci. Paris, sér. IIc* **2000**, *3*, 131.

(5) Costes, J.-P.; Dahan, F.; Dupuis, A.; Laurent, J.-P. *J. Inorg. Chem.* **2000**, *39*, 169.

interaction between  $\text{Ln}^{\text{III}}$  and the other paramagnetic species.

To better understand the magnetic interaction between  $\text{Ln}^{\text{III}}$  and  $\text{Cu}^{\text{II}}$ , we developed an experimental methodology allowing the intrinsic rare earth ion magnetic properties in its ligand field to be set free. Our approach is to compare the  $\chi_{\text{M}}T$  versus  $T$  curves,  $\chi_{\text{M}}$  being the molar magnetic susceptibility and  $T$  the temperature, for two series of compounds  $\{\text{Ln}_2[\text{M}(\text{opba})_3] \cdot \text{S}\}$ , where  $\text{M} = \text{Cu}^{\text{II}}$  or  $\text{Zn}^{\text{II}}$ , opba stands for *o*-phenylenebis(oxamato), and  $\text{S} =$  solvent molecules. In our preceding papers, it has been shown through wide-angle X-ray scattering (WAXS) experiments that all these compounds present the same infinite ladder-like motif<sup>6</sup> as that previously described for an X-ray diffraction study of the  $\{\text{Tm}_2[\text{Cu}(\text{opba})_3] \cdot 4\text{H}_2\text{O} \cdot 10\text{DMF}\}$  compound.<sup>7</sup> The magnetic properties of the series with  $\text{M} = \text{Cu}^{\text{II}}$  result in the magnetic behavior of the Ln ions and the magnetic interaction between Ln and Cu ions. In the other series, with  $\text{M} = \text{Zn}^{\text{II}}$ , only the intrinsic magnetic properties arising from the thermal depopulation of the Stark sublevels of Ln ions are measured. The difference of the  $\chi_{\text{M}}T$  products of these two series, for a given  $\text{Ln}^{\text{III}}$ , give information about the nature of the magnetic interaction between  $\text{Ln}^{\text{III}}$  and  $\text{Cu}^{\text{II}}$  ions. By this method we have shown that, in these polymeric compounds, the  $\text{Dy}^{\text{III}}-\text{Cu}^{\text{II}}$  and  $\text{Tb}^{\text{III}}-\text{Cu}^{\text{II}}$  interactions are ferromagnetic like those for  $\text{Gd}^{\text{III}}-\text{Cu}^{\text{II}}$ . Perhaps the  $\text{Tm}^{\text{III}}-\text{Cu}^{\text{II}}$  interactions are also ferromagnetic. For the other rare earth ions, the interaction with  $\text{Cu}^{\text{II}}$  is not ferromagnetic; it is either not detectable or antiferromagnetic.<sup>8</sup>

Recently, molecular compounds containing  $\text{Gd}^{\text{III}}$  and transition metal ions different from  $\text{Cu}^{\text{II}}$  were described.<sup>9</sup> The magnetic interaction between  $\text{Gd}^{\text{III}}$  and paramagnetic transition metal ions has always been described as ferromagnetic, except the Costes's compound quoted above. Along this line, we applied our experimental approach to give more information on magnetic interactions between  $\text{Ln}^{\text{III}}$  and  $\text{Ni}^{\text{II}}$  ions.

We synthesized a third series of  $\{\text{Ln}_2[\text{M}(\text{opba})_3]\}$  compounds with  $\text{M} = \text{Ni}^{\text{II}}$ . All these compounds crystallize poorly, and we used WAXS technique to obtain structural information. The three series have similar extended structures consisting of ladder-type motifs, whatever the Ln and the 3d ions are.<sup>6</sup> However, the 3d ion site can adopt square planar or a square pyramidal or octahedral geometry, depending on zero, one or two solvent molecules, respectively. This change of geometry is of great importance for the magnetic properties in the case of Ni compounds. Actually, it is well-known that Ni complexes in which the metallic center is in a square planar environment are diamagnetic whereas Ni com-

plexes with square pyramidal or octahedral symmetry are paramagnetic. To get more information on the Ni site in the  $\{\text{Ln}_2[\text{Ni}(\text{opba})_3]\}$  series, EXAFS experiments have been performed. Then, the magnetic properties have been measured and compared with those of the  $\{\text{Ln}_2[\text{Zn}(\text{opba})_3] \cdot \text{S}\}$  compounds. This gave access to the nature of the magnetic interaction between  $\text{Ln}^{\text{III}}$  and  $\text{Ni}^{\text{II}}$  ions. These results will be discussed in relation to those obtained for compounds involving  $\text{Ln}^{\text{III}}$  and  $\text{Cu}^{\text{II}}$  ions.

## Experimental Section

**Syntheses.** The compounds were obtained according to the procedures described in ref 6. An important point to mention here is the color of powdered compounds. We noticed that the  $\{\text{Ln}_2[\text{Ni}(\text{opba})_3] \cdot \text{S}\}$  compounds color depended on the batch syntheses. While the  $(\text{NBu}_4)_2\text{Ni}(\text{opba})$  precursor compound is invariably orange, the polymeric compounds displayed colors ranging from orange to pale green.

**Structural Studies EXAFS Study.** Round pellets were prepared by cold pressing the powder sample mixed with organic binder. The spectra were collected in transmission mode at the Ni K absorption edge on the XAS13 spectrometer at the French synchrotron facility LURE (Orsay). Four samples were studied. The two  $\text{Ln}_2[\text{Ni}(\text{opba})_3] \cdot \text{S}$  compounds came from two different batch syntheses: the first one noted  $\text{Ni}_3\text{Pr}_2\text{-g}$  is pale green and the other one noted  $\text{Ni}_3\text{Pr}_2\text{-o}$  is orange. Two reference Ni complexes with well-defined coordination schemes of the central nickel atom were also characterized:  $[\text{Ni}(\text{en})_3]\text{-Cl}_2$  (noted  $\text{Ni-O}_h$ ) and  $(\text{NMe}_4)_2\text{Ni}(\text{opba})$  (noted  $\text{Ni-SQP}$ ) with an octahedral and a square planar coordination Ni sphere, respectively. Data were analyzed using classic procedures (background subtraction, Fourier transform). Further treatments involving Fourier filtering and least-squares refinement of parameters have been performed.

**WAXS Study.** All the samples were sealed in thin-walled Lindemann glass capillaries of 1.5 mm in diameter. The X-ray intensity scattered by the sample irradiated with graphite-monochromatized molybdenum  $\text{K}\alpha$  radiation ( $\lambda = 0.71069 \text{ \AA}$ ) was obtained using a specific two-axis diffractometer. Then, 457 measurements sampled for equidistant  $s$  values ( $s = 4\pi(\sin \theta/\lambda)$ ;  $\Delta s = 0.035 \text{ \AA}^{-1}$ ) were collected in the  $0^\circ$ – $65^\circ$   $\theta$  range. Measurement of an empty Lindemann capillary was carried out exactly under the same conditions. The total scattered intensity (sample + capillary) was corrected for capillary contribution by spectra subtraction, taking into account absorption from the sample. The effects of polarization and self-absorption are taken into account.<sup>10</sup> Normalization was performed using Norman and Krogh–Moe's method.<sup>11</sup> The atomic scattering factors were taken from Cromer and Waber.<sup>12</sup> The reduced experimental radial distribution function (RDF) was calculated similar to that given in ref 13. Theoretical structural models were built up using the CERIOUS2 program.<sup>14</sup> The theoretical RDF was computed from the structural models by Fourier transform of the theoretical intensities calculated using the Debye's formula.<sup>15</sup>

**Magnetic Measurements.** These were carried out with a Quantum Design MPMS-5S SQUID magnetometer working

(6) Kahn, M. L.; Verelst, M.; Lecante, P.; Mathonière, C.; Kahn, O. *Eur. J. Inorg. Chem.* **1999**, 527.

(7) Oushorn, R. L.; Boubekour, K.; Batail, P.; Guillou, O.; Kahn, O. *Bull. Soc. Chim.* **1996**, 133, 777.

(8) Kahn, M. L.; Mathonière, C.; Kahn, O. *Inorg. Chem.* **1999**, 38, 3692.

(9) (a) Archibald, S. J.; Blake, A. J.; Parsons, S.; Schröder, M.; Winpenny, R. E. P. *J. Chem. Soc., Chem. Commun.* **1997**, 173. (b) Brechin, E. K.; Harris, S. G.; Parsons, S.; Winpenny, R. E. P. *J. Chem. Soc., Chem. Commun.* **1997**, 1665. (c) Goodgame, D. M. L.; Menzer, S.; Ross, A. T.; Williams, D. J. *J. Chem. Soc., Chem. Commun.* **1994**, 2605. (d) Costes, J.-P.; Dupuis, A.; Laurent, J.-P. *J. Chem. Soc., Dalton Trans.* **1998**, 735. (e) Benelli, C.; Murrie, M.; Parsons, S.; Winpenny, R. E. P. *J. Chem. Soc.* **1999**, 4125.

(10) Air scattering was small enough to be neglected.

(11) (a) Norman, N. *Acta Crystallogr.* **1957**, 10, 370. (b) Krogh-Moe, *Acta Crystallogr.* **1956**, 9, 951.

(12) Cromer, D.; Waber, T. J. *International Tables for X-ray Crystallography*; Kynoch Press: Birmingham, 1974; Vol. 4.

(13) See for example: (a) Mosset, A.; Lecante, P.; Galy, J. *Philos. Magn. B* **1982**, 46, 137. (b) Burian, A.; Lecante, P.; Mosset, A.; Galy, J. *J. Non-Cryst. Solids* **1987**, 90, 633. (c) Laberty, C.; Verelst, M.; Lecante, P.; Mosset, A.; Alphonse, P.; Rousset, A. *J. Solid State Chem.* **1997**, 129, 271. (d) Verelst, M.; Sommier, L.; Lecante, P.; Mosset, A.; Kahn, O. *Chem. Mater.* **1998**, 10, 980. (e) Cador, O.; Mathonière, C.; Kahn, O.; Costes, J.-P.; Verelst, M.; Lecante, P. *Inorg. Chem.* **1999**, 38, 2643.

(14) CERIOUS2 molecular simulation program is supplied by BIOSYM technologies and runs on an Indy Silicon Graphics workstation.

(15) Debye, P. *Ann. Phys.* **1915**, 46, 809.

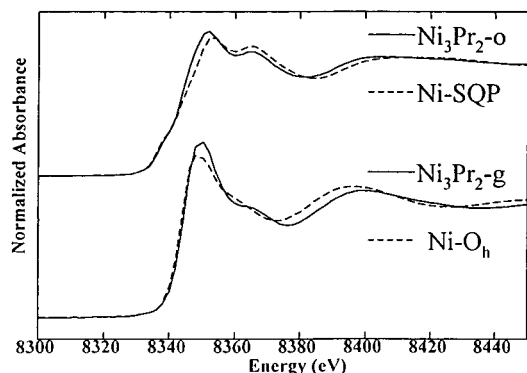


**Figure 1.** Near-edge absorption spectra (top: solid,  $Ni_3Pr_2-o$ ; dashed,  $Ni-SQP$ ; bottom: solid,  $Ni_3Pr_2-g$ ; dashed,  $Ni-O_h$ ).

in the dc mode. The measurements were performed in the 2–300 K temperature range, with a magnetic field of 1000 Oe. All the compounds are highly solvated with dimethyl sulfoxide and water molecules, and the exact number of noncoordinated solvent molecules is not known accurately. Therefore, there is some uncertainty in the molecular weight of the compounds and consequently in the molar magnetic susceptibilities. To overcome this difficulty, it was assumed that for each compound the high-temperature limit of  $\chi_M T$  was reached at 300 K, and the experimental  $\chi_M T$  was rescaled accordingly when necessary. Moreover, as mentioned in the Introduction, the proportion of Ni paramagnetic sites in polymeric compounds is also unknown. The rescaling of the  $\chi_M T$  curves for the Ni compounds is erroneous but our purpose does not concern the absolute values of the  $\chi_M T$  products but only the shape of the curves, which is correct.

## Results

**EXAFS Study.** In Figure 1 is presented the near-edge absorption spectra for the four compounds:  $Ni-O_h$ ,  $Ni-SQP$ ,  $Ni_3Pr_2-o$ , and  $Ni_3Pr_2-g$ . For all spectra, the linear pre-edge was extrapolated and subtracted before scaling to unity. Reference compounds exhibit characteristics known to reflect local symmetry of the absorber: marked details inside the edge (below 8340 eV) for  $Ni-SQP$  and a more apparent white line for  $Ni-O_h$ . A comparison of these two reference spectra with  $Ni_3Pr_2-o$  and  $Ni_3Pr_2-g$  clearly shows that in the former the Ni sites are mostly square planar and in the latter the Ni sites are mostly octahedral. The absorption functions were extracted. Fourier transform, taking into account phase shift for Ni–O interaction, was performed using the curved-wave single scattering phase and amplitude functions published by MacKale.<sup>16</sup> These corrected functions are displayed in Figure 2. Here again, each  $Ni_3Pr_2$  compound is closely connected to one reference compound. Applying Lee and Beni criterion,<sup>17</sup> nearest neighbor distances are found: 1.85 Å for  $Ni-SQP$ , 1.86 Å for  $Ni_3Pr_2-o$ , 2.11 Å for  $Ni-O_h$ , and 2.06 Å for  $Ni_3Pr_2-g$ . It is therefore demonstrated that the Ni coordination in  $Ni_3Pr_2-o$  is very close to the one in  $Ni-SQP$ . Indeed, the first distances are close; shapes and relative amplitudes are very similar for the peaks observed between 1.4 and 4 Å. A less obvious scheme occurs for  $Ni_3Pr_2-g$ . The first distance is consistent with a square planar environment but the first peak is much broader than that in  $Ni-O_h$ . Moreover, differences are observed be-

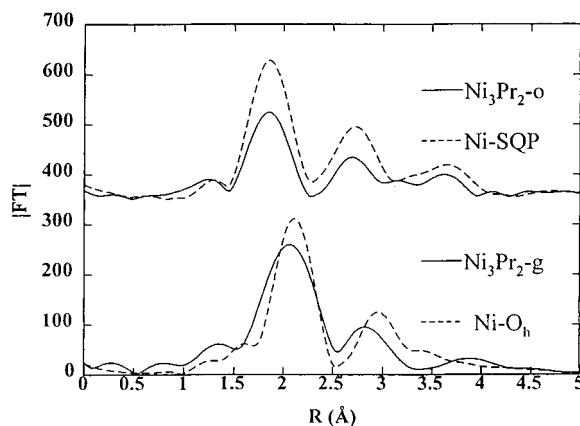


**Figure 2.** Modulus of corrected Fourier transforms (top: solid,  $Ni_3Pr_2-o$ ; dashed,  $Ni-SQP$ ; bottom: solid,  $Ni_3Pr_2-g$ ; dashed,  $Ni-O_h$ ).

tween the two patterns. Filtering was performed in real space on the uncorrected Fourier transforms to extract and then to back-transform the first and second peak for each compound. The related  $\chi_{exp}(k)$  functions were used to perform a least-squares refinement process to minimize the  $R$  factor, according to

$$R = \left\{ \sum_i [k_i^3 \chi_{exp}(k_i) - k_i^3 \chi_{fit}(k_i)]^2 / \sum_i [k_i^3 \chi_{exp}(k_i)]^2 \right\}^{1/2}$$

where  $k^2 = 8\pi^2 m(E - E_0)/h^2$ ,  $m$  is the mass of the electron,  $h$  is Planck's constant,  $E_0$  is the threshold energy, and  $\chi_{fit}(k)$  defines the theoretical amplitude in the single-scattering approximation,

$$\chi_{fit}(k) = S_i \sum_j N_j F_j(k) \exp(-2k^2 \sigma_j^2) \exp\left(\frac{-2r_j}{\lambda_j}\right) \frac{\sin[2kr_j + \Phi_{ij}(k)]}{kr_j^2}$$

where  $S_i$  is an amplitude scaling factor,  $F_j$  is the backscattering amplitude from  $N_j$  neighboring atoms of the  $j$ th type at a distance  $r_j$  from the absorbing atom  $i$ ,  $\lambda_j$  is the electron mean free path approximated by  $[(3.913/k)^4 + k]/0.95$ ,<sup>18</sup>  $\sigma_j$  is the standard deviation of the interatomic distance, and  $\Phi_{ij}$  is the total phase shift. MacKale functions were also used for  $F_j$  and  $\Phi_{ij}$ . Values are given in Table 1. To reduce the number of parameters and avoid correlations, only one set of parameters was refined for the Ni–O and Ni–N interactions related to the first peak, except for  $Ni_3Pr_2-o$ . In Figure 3 is observed a global good agreement. If not perfect, it leaves no ambiguity on the choice of the valid model for each compound, and it could be obtained with a reduced number of simultaneously refined parameters. In the case of the  $Ni_3Pr_2-g$  compound, a less satisfying fit is obtained (higher value for the agreement factor, and mostly low value for the scale factor). This might indicate that the proposed model, mostly correct, does not completely describe the real environment of the Ni ion in  $Ni_3Pr_2-g$ .

**WAXS Study.** Although the EXAFS study has clearly revealed that coordination of Ni spheres is different in  $Ni_3Pr_2-o$  and  $Ni_3Pr_2-g$  compounds, WAXS investigation

(16) MacKale, G.; Veal, B. W.; Paulikas, A. P.; Chan, S. K.; Knapp, G. S. *J. Am. Chem. Soc.* **1988**, *110*, 3763.

(17) Lee, P. A.; Beni, G. *Phys. Rev. B* **1977**, *15*, 2862.

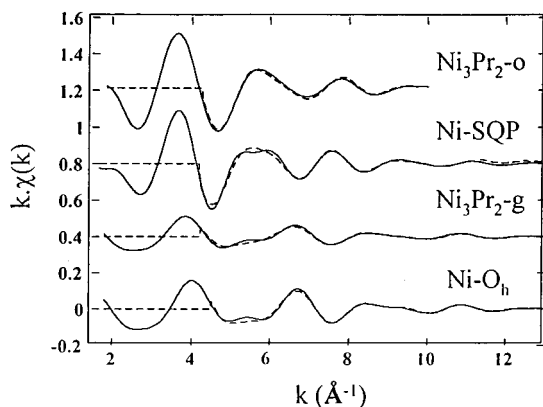
(18) Teo, B. K. *EXAFS: Basic Principles and Data Analysis*; Springer: Berlin, 1986.



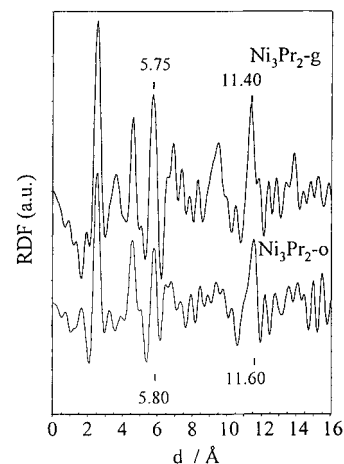
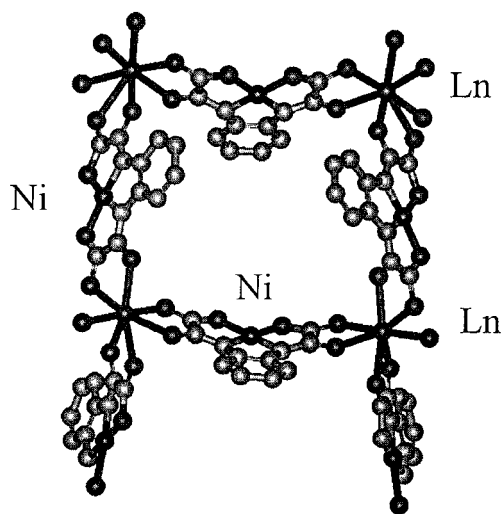
**Table 1. Best-Fit Parameters of the First Coordination Sphere of the EXAFS Data<sup>a</sup>**

compounds	<i>N</i>	<i>r</i> (Å)	$\sigma$ (Å)	$\Delta E$ (eV)
Ni- <i>O<sub>h</sub></i> Interaction				
Ni-O	4	2.124	0.0853	-2.35
Ni-N	2	2.124	0.0853	-2.35
Ni-C	6	2.976	0.0815	-2.35
<i>R</i> = 0.0267	scale factor = 1.0294			
Ni <sub>3</sub> Pr <sub>2</sub> -g Interaction				
Ni-O	4	2.028	0.0624	-2.98
Ni-N	2	2.174	0.0507	-2.98
Ni-C	6	2.891	0.0800	-2.98
<i>R</i> = 0.0257	scale factor = 0.8478			
Ni-SQP Interaction				
Ni-O	2	1.841	0.0743	-10.7
Ni-N	2	1.841	0.0743	-10.7
Ni-C	4	2.775	0.0398	-10.7
Ni-C	2	2.687	0.0100	-10.7
<i>R</i> = 0.0227	scale factor = 0.782			
Ni <sub>3</sub> Pr <sub>2</sub> -o Interaction				
Ni-O	2	1.836	0.0624	-18.3
Ni-N	2	1.836	0.0624	-18.3
Ni-C	6	2.708	0.0548	-18.3
<i>R</i> = 0.0466	scale factor = 0.401			

<sup>a</sup> For all fits, *N* values were fixed. All other parameters were allowed to vary simultaneously. The Minuit program from CERN was used for the least-squares refinement procedure. Initial values for  $\Delta E$  were obtained from Lee and Beni's criterion and were very close to the refined values. The large discrepancy for  $\Delta E$  is caused by the method used to extract  $E_0$ , which is biased by the shape of the edge. As a consequence, two sets of  $\Delta E$  values (small and large) can be observed for the two geometries of the Ni site (*O<sub>h</sub>* and SQP, respectively).

**Figure 3.** Absorption functions for the first two peaks in Fourier transform (solid lines are experimental functions and dashed lines are computed according to refined parameters).

shows that long-range order remains almost unchanged in the two compounds. The RDFs shown in Figure 4 clearly show that the ladder characteristics are very similar in both cases. Small differences in the RDF peaks corresponding to the Ni...Pr and Pr...Pr distances are observed: they are respectively found as 5.75 and 11.40 Å in Ni<sub>3</sub>Pr<sub>2</sub>-o and 5.80 and 11.60 Å in Ni<sub>3</sub>Pr<sub>2</sub>-g. The ladder shape is not much affected by the Ni coordination sphere. The absence of solvent molecules in the apical position in the Ni coordination sphere causes only a weak shortening of Ni...ligand(opba) distances (2.07 Å in Ni<sub>3</sub>Pr<sub>2</sub>-g and 1.88 Å in Ni<sub>3</sub>Pr<sub>2</sub>-o). Consequently, the length of the upright is different (11.40 Å in Ni<sub>3</sub>Pr<sub>2</sub>-o and 11.60 Å in Ni<sub>3</sub>Pr<sub>2</sub>-g). Note that in the two compounds the Ni(opba) brick is nearly flat

**Figure 4.** Experimental RDF for Ni<sub>3</sub>Pr<sub>2</sub>-g (top) and Ni<sub>3</sub>Pr<sub>2</sub>-o (bottom).**Figure 5.** Simulated structure of Ni<sub>3</sub>Pr<sub>2</sub> as deduced from the WAXS and EXAFS studies with the Ni site in square planar geometry.

because the Pr...Pr distances are very close to the double of the Pr...Ni ones. Although the EXAFS study revealed Ni...ligand distances noticeably different in the two-coordination mode ( $\delta d/d = 9\%$ ), we were rather astonished that the main ladder parameters are so weakly affected by this coordination mode of the Ni site ( $\delta d/d = 2\%$ ). This effect has been confirmed by several WAXS studies, done on samples coming from different syntheses batches. However, the intensity of this effect is not reproducible. Thus, we concluded that the coordination sphere of the Ln ion in these compounds could evolve.

Using EXAFS and WAXS results, a ladder motif simulation has been attempted. Figure 5 shows the structure simulated for Ni<sub>3</sub>Pr<sub>2</sub>-o using CERIUS2 software, whereas Figure 6 compares experimental and calculated WAXS spectra in both direct (RDF) and reciprocal (reduced intensity) spaces. Even if the fitting procedure is not absolutely perfect, both experimental and calculated spectra are close enough to strongly suggest that the proposed model is the good one. The minor discrepancy can be interpreted in the sense that the real structure is not so symmetric as the computed one, possibly because of the presence of solvent molecules outside the ladder motif.

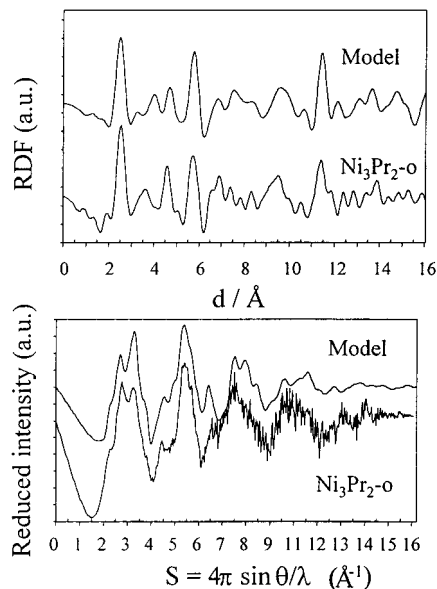


**Figure 6.** Comparison of the calculated and experimental RDF (top) and reduced intensities (bottom) for the model and  $Ni_3Pr_2 \cdot o$ .

**Magnetic Properties.** The EXAFS studies clearly demonstrated that the Ni site in our compounds adopt two different coordination modes. In the  $Ni_3Ln_2 \cdot o$  series, the Ni site is planar and then diamagnetic. No significant magnetic interaction is expected in this series. For the  $Ni_3Ln_2 \cdot g$  series, the Ni sites adopt mostly an octahedral geometry. The Ni ion completes its coordination sphere of the opba ligand with solvent molecules  $S$  ( $S = \text{DMSO}$  or  $\text{H}_2\text{O}$ ) and then becomes magnetic. The exact proportion of the Ni magnetic sites is unknown and the information deduced in this work is only qualitative. The WAXS studies have shown that the structure of the compounds is the same whatever the  $Ln^{III}$  and  $M^{II}$  ions are. Consequently, our experimental method allows us to determine the nature of the magnetic interaction in those compounds. In the following we present the magnetic properties of the  $Ni_3Ln_2 \cdot g$  (noted as  $Ni_3Ln_2$  in the following) series in comparison with those of the  $Zn_3Ln_2$  series.

Our experimental methodology is explained in detail in ref 8. It consists of plotting for each  $Ln^{III}$  the  $\Delta\chi_M T$  versus  $T$  curves obtained by the difference of two  $\chi_M T$  curves: one for  $Ni_3Ln_2$  compounds and the other for  $Zn_3Ln_2$  compounds. The resulting  $\Delta\chi_M T$  curve is indicative of the nature of the interaction between  $Ni^{II}$  and  $Ln^{III}$  ions. For the extended structures studied in this paper, three distinct behaviors are expected. If  $\Delta\chi_M T$  is increasing continuously when the temperature decreases, the interaction between  $Ln^{III}$  and  $Ni^{II}$  ions is ferromagnetic. If the interaction between  $Ln^{III}$  and  $Ni^{II}$  ions is antiferromagnetic, two variations of  $\Delta\chi_M T$  plots may be observed when the temperature decreases: a monotonic decrease if the magnetic moments in interaction are equal or a decrease followed by an increase in the low-temperature range showing a minimum if the magnetic moments in interaction are noncompensating.

We have measured the magnetic properties of eight couples of compounds, each couple being  $Ni_3Ln_2$  and  $Zn_3Ln_2$  compounds with  $Ln = \text{Ce}, \text{Pr}, \text{Nd}, \text{Gd}, \text{Tb}, \text{Dy}, \text{Ho},$  and  $\text{Er}$ . Three types of  $\Delta\chi_M T$  plots were obtained

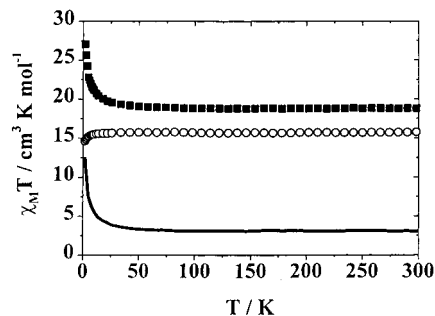


**Figure 7.**  $\chi_M T$  versus  $T$  curves for  $Ni_3Gd_2 \cdot g$  (■) and  $Zn_3Gd_2$  (○) and  $\Delta\chi_M T$  (solid line).

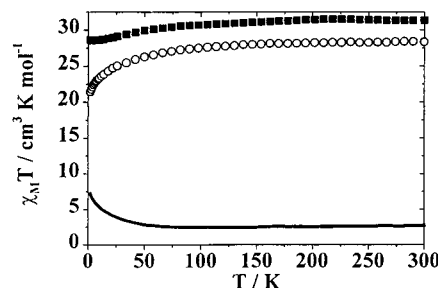


**Figure 8.**  $\chi_M T$  versus  $T$  curves for  $Ni_3Dy_2 \cdot g$  (■) and  $Zn_3Dy_2$  (○) and  $\Delta\chi_M T$  (solid line).

and we will restrict ourselves in this paper to typical examples.

The Gd compounds are cases validating our experimental method to some extent. In fact, the  $Gd^{III}$  has a pure spin ground-state  $^8S_{7/2}$  corresponding to a unique Stark component. The  $\chi_M T$  curve for  $Zn_3Gd_2$  corresponds down to 9 K to the Curie law anticipated for two isolated  $Gd^{III}$  ions. As  $T$  is lowered further, the decrease of  $\chi_M T$  might be due to intra- and/or interladder effects. Let us note that the intra- and/or interladder interactions in  $Ni_3La_2$  involving the diamagnetic  $La^{III}$  are weak but observed at low temperatures:  $\chi_M T$  is constant from 300 to 12 K and decreases below 12 K. For  $Ni_3Gd_2$ , the deviation of the magnetic behavior with respect to the Curie law is due to  $Gd^{III}-Ni^{II}$  interaction, and  $\chi_M T$  is constant down to 50 K and then increases rapidly (Figure 7). The  $\Delta\chi_M T = (\chi_M T)_{Ni_3Gd_2} - (\chi_M T)_{Zn_3Gd_2}$  plot is therefore constant down to 50 K and then increases rapidly as  $T$  is lowered. This profile for  $\Delta\chi_M T$  is characteristic of ferromagnetic correlation within the  $Ni_3Gd_2$  compound.

Let us consider now Ln ions with a first-order momentum. In Figure 8 is presented the Dy case, where the  $\Delta\chi_M T$  product increases monotonically when the temperature decreases. The  $Tb^{III}$  case displays a similar  $\Delta\chi_M T$  plot.  $Dy^{III}$  has a  $^6H_{15/2}$  ground state. In the low-symmetry site, this state is split into eight Stark components by the crystal field, each of them being a Kramers doublet. As the temperature is decreased, a progressive depopulation of excited Stark components occurs, and at 2 K only the ground Kramers doublet is populated. As shown in Figure 8, the  $\chi_M T$  plot for  $Ni_3Dy_2$  is different than that of  $Ni_3Gd_2$ : when the temperature is lowered, the  $\chi_M T$  product first decreases and then increases at low temperature. The decreasing of  $\chi_M T$  is essentially due to the thermal depopulation of excited Stark components, as illustrated for  $Zn_3Dy_2$  compounds. At low temperature, the magnetic proper-

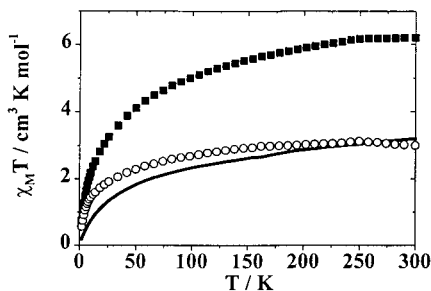


**Figure 9.**  $\chi_M T$  versus  $T$  curves for  $\text{Ni}_3\text{Pr}_2\text{-g}$  (■) and  $\text{Zn}_3\text{Pr}_2$  (○) and  $\Delta\chi_M T$  (solid line).

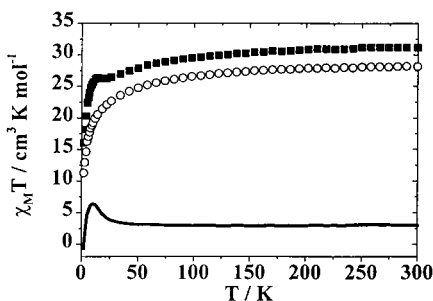


**Figure 10.**  $\chi_M T$  versus  $T$  curves for  $\text{Ni}_3\text{Ho}_2\text{-g}$  (■) and  $\text{Zn}_3\text{Ho}_2$  (○) and  $\Delta\chi_M T$  (solid line).

ties of  $\text{Ni}_3\text{Dy}_2$  are dominated by the interaction in Dy–Ni pairs. As emphasized by the  $\Delta\chi_M T$  plots, this interaction is ferromagnetic.

Figure 9 represents the Pr case. The Ce, Nd, and Er cases are analogous.  $\text{Pr}^{\text{III}}$  with a  $^3\text{H}_4$  ground state is not a Kramers ion. It means that the crystal field alone can resolve degeneracy to give a nonmagnetic ground state.<sup>19</sup> For  $\text{Ni}_3\text{Pr}_2$  and  $\text{Zn}_3\text{Pr}_2$ ,  $\chi_M T$  decreases continuously when the temperature decreases. At 2 K the  $\chi_M T$  value for  $\text{Zn}_3\text{Pr}_2$  is  $0.18 \text{ emu K mol}^{-1}$ , suggesting that the compound is weakly magnetic at this temperature. The  $\Delta\chi_M T$  plot also decreases slightly when the temperature is cooled to 50 K and more rapidly down to 2 K. Clearly, the magnetic interaction between Pr and Ni is not ferromagnetic. But the low-temperature behavior is difficult to interpret because some intraladder  $\text{Ni}^{\text{II}}\text{Ni}^{\text{II}}$  and/or interladder interactions may superimpose to an intraladder antiferromagnetic  $\text{Pr}^{\text{III}}\text{--Ni}^{\text{II}}$  interaction.

Figure 10 illustrates the Ho case.  $\text{Ho}^{\text{III}}$  has a  $^5\text{I}_8$  ground state and is another non-Kramers ion. Whereas the  $\chi_M T$  plot for  $\text{Zn}_3\text{Ho}_2$  decreases monotonically when the temperature decreases, the  $\chi_M T$  plot for  $\text{Ni}_3\text{Ho}_2$  decreases first, reaches a plateau between 25 and 10 K, and finally decreases at lower temperatures. The  $\Delta\chi_M T$  plot is constant when the temperature decreases down to 25 K, then increases when  $T$  is lowered to 11 K, and finally decreases when  $T$  is lowered further. The increase of  $\Delta\chi_M T$  between 25 and 11 K means that the global moment of the  $\text{Ni}_3\text{Ho}_2$  compound is superior to the isolated moments. This seems to indicate ferromagnetic interaction between  $\text{Ho}^{\text{III}}$  and  $\text{Ni}^{\text{II}}$  ions. The diminution of  $\Delta\chi_M T$  at lower temperatures might have the same origins as those mentioned in  $\text{Ni}_3\text{La}_2$ .

## Discussion and Concluding Remarks

In this work we demonstrate that our experimental approach is of general interest for determining the nature of magnetic interaction between the  $\text{Ln}^{\text{III}}$  and other paramagnetic species in molecular compounds. The coordination chemistry allows us to obtain easily two different series of compounds: one with local  $\text{Ln}^{\text{III}}$  magnetic properties and the second with magnetic properties resulting from Ln ion and interaction between an Ln ion and other magnetic species. The key point of this approach is the knowledge of the structures of studied compounds. Here, no single crystals were available for X-ray diffraction. EXAFS and WAXS techniques are known to obtain structural details for such amorphous molecular magnetic compounds. The first technique gives local information whereas the second gives information about the extended network. In this study, we have shown that even if the local geometry of the  $\text{Ni}^{\text{II}}$  ion changes, the global structure is still the same for all the compounds.

Our experimental method allows us to conclude without ambiguity that a ferromagnetic interaction takes place between  $\text{Ln}^{\text{III}}$  and  $\text{Ni}^{\text{II}}$ , for  $\text{Ln}^{\text{III}}=\text{Gd}^{\text{III}}, \text{Tb}^{\text{III}}, \text{Dy}^{\text{III}}$ , and perhaps  $\text{Ho}^{\text{III}}$ . As we never observed the minimum in  $\Delta\chi_M T$  plots at low temperatures, an antiferromagnetic interaction between  $\text{Ln}^{\text{III}}$  and  $\text{Ni}^{\text{II}}$ , for  $\text{Ln}^{\text{III}}=\text{Ce}^{\text{III}}, \text{Pr}^{\text{III}}, \text{Nd}^{\text{III}}$ , and  $\text{Er}^{\text{III}}$  may exist, but must be weak. If not, a minimum in  $\Delta\chi_M T$  curves may appear for  $T > 2 \text{ K}$ , except in the case of accidentally compensating spin sublattices.<sup>20</sup> The general observed behavior excludes this situation. We prefer to say that, in these cases, the  $\text{Ln}^{\text{III}}\text{--Ni}^{\text{II}}$  interaction is weak and not ferromagnetic. We may propose with caution an antiferromagnetic interaction.

This experimental approach has already been used by us for the similar  $\text{Cu}_3\text{Ln}_2$  series<sup>8</sup> and by other colleagues for molecular  $\text{CuLn}$  finite compounds.<sup>21</sup> In Table 2 are reported the results of  $\text{CuLn}$  pairs and those obtained by us, on extended  $\text{LnNi}$  and  $\text{LnCu}$  compounds. If we do not taken into account our difficulties to determine properly the magnetic interaction in the case of weak interactions, a general trend emerges. Clearly, for each  $\text{Ln}^{\text{III}}$ , similar conclusions can be drawn, whatever the other 3d paramagnetic species. This suggests some general aptitude for light  $\text{Ln}^{\text{III}}$  ( $\text{Ln} = \text{Ce} \dots \text{Eu}$ ) to interact in an antiferromagnetic fashion with other 3d paramagnetic species whereas the heavy  $\text{Ln}^{\text{III}}$  ( $\text{Ln} = \text{Gd} \dots \text{Ho}$ ) interacts in a ferromagnetic fashion with other 3d paramagnetic species. The cases of  $\text{Er}^{\text{III}}, \text{Tm}^{\text{III}}$ , and  $\text{Yb}^{\text{III}}$  are not yet well documented to make a conclusion. Recently, the same trends have been observed for  $\text{Ln}^{\text{III}}$  ions in magnetic interaction with organic ligands.<sup>22</sup> These conclusions are in line with the predictions of Kahn et al.<sup>3</sup> As sketched in Table 2, this model suggests that the spin momenta of  $\text{Ln}^{\text{III}}$  and other paramagnetic species are parallel to each other, according to the mechanisms quoted in the Introduction. For light (respectively, heavy)  $\text{Ln}^{\text{III}}$ , angular and spin momenta

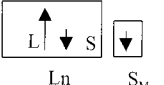
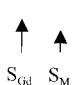
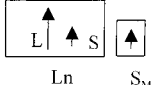
(20) Kahn, O.; Guillou, O.; Oushoorn, R. L.; Drillon, M.; Rabu, P.; Boubekour, K.; Batail, P. *New J. Chem. Eur. J.* **1995**, *19*, 655.

(21) Costes, J.-P.; Dahan, F.; Dupuis, A.; Laurent, J.-P. *Chem. Eur. J.* **1998**, *4*, 1616.

(22) Kahn, M. L.; Sutter, J.-P.; Gohlen, S.; Guionneau, P.; Ouahab, L.; Kahn, O.; Chasseau, D. *J. Am. Chem. Soc.* **2000**, *122*, 3413.

(19) Carlin, R. L. *Magnetochemistry*; Springer-Verlag: Berlin, 1986.

**Table 2. Nature of Magnetic Interaction between  $Ln^{III}$  and  $M^{II}$  Ions Determined by the Experimental Method Described in the Text<sup>a</sup>**

Compound	Ln	Ce	Pr	Nd	Sm	Eu	Gd	Tb	Dy	Ho	Er	Tm	Yb						
$Ni_3Ln_2 \cdot g$		af	af	af	af	af	F	F	F	f									
$Cu_3Ln_2$		af	af	af	af	af	F	F	F			f							
$CuLn$ pairs <sup>21</sup>		AF		AF	AF		F	F	F	F	F	AF							
Kahn's prediction		 Ln $S_M$					 $S_{Gd}$ $S_M$		 Ln $S_M$										
		Overall AF interaction									Overall F interaction								

<sup>a</sup> AF, antiferromagnetic interaction; F, ferromagnetic interaction; af, proposed antiferromagnetic interaction; f, proposed ferromagnetic interaction.

are antiparallel (respectively, parallel). The parallel alignment of the  $Ln^{III}$  and other paramagnetic species spin momenta lead to an overall antiferromagnetic (respectively, ferromagnetic) interaction.

To sum up, ferromagnetic interactions were obtained in molecular compounds in  $Gd^{III}-M$ ,  $Tb^{III}-M$ , and  $Dy^{III}-M$  pairs for  $M = Cu^{II}$ ,  $Ni^{II}$  and in  $Ho^{III}-Ni^{II}$  and  $Ho^{III}-Cu^{II}$  in the case of finite bimetallic compounds irrespective of the pair geometry. This is very different

from what happened in 3d–3d pairs in which a strict orthogonality of magnetic orbitals is often required to get a ferromagnetic interaction. This last condition is very restrictive because of the low symmetry of molecular compounds. If the  $Ln^{III}$  ion is involved, the ferromagnetic interaction seems easy to obtain but the price to pay is a weaker magnetic interaction.

CM001042P